ACS NANO

www.acsnano.org

ARTICLE

Photoluminescence Switching Effect in a Two-Dimensional Atomic Crystal

Zheng Sun,*,# Ke Xu,# Chang Liu,# Jonathan Beaumariage, Jierui Liang, Susan K. Fullerton-Shirey, Zhe-Yu Shi, Jian Wu, and David Snoke

Cite This: *ACS Nano* 2021, 15, 19439–19445

Read Online

ACCESS | Metrics & More | Article Recommendations | Supporting Information

ABSTRACT: **Two-dimensional materials are an emerging class of materials with a wide range of electrical and optical properties and potential applications. Single-layer structures of semiconducting transition metal dichalcogenides are gaining increasing attention for use in field-effect transistors. Here, we report a photoluminescence switching effect based on single-layer WSe_2 transistors. Dual gates are used to tune the photoluminescence intensity. In particular, a side-gate is utilized to control the location of ions within a solid polymer electrolyte to form an electric double layer at the interface of electrolyte and WSe_2 and induce a vertical electric field. Additionally, a back-gate is used to apply a second vertical electric field. An on−off ratio of the light emission up to 90 was observed under constant pump light intensity. In addition, a blue shift of the photoluminescence line up to 36 meV was observed. We attribute this blue shift to the decrease of exciton binding energy due to the change of nonlinear in-plane dielectric constant and use it to determine the third-order off-diagonal susceptibility $\chi^{(3)} = 3.50 \times 10^{-19}$ m^2/V^2.**

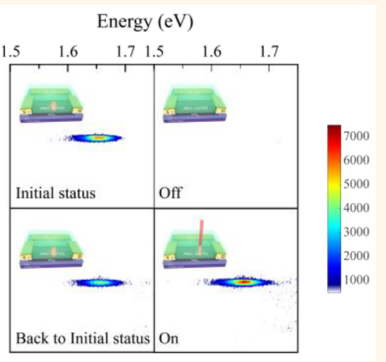

KEYWORDS: *photoluminescence switching effect, two-dimensional materials, dual gates, blue shift, susceptibility*

Low-dimensional semiconducting transition metal dichalcogenides (TMDs), with MX_2 stoichiometry, where M is a transition metal element from group VI (M = Mo, W) and X is a chalcogen (X = S, Se), have emerged as promising materials, offering complementary characteristics to graphene for electronics, photonics, and optoelectronics applications because of their unusual electrical and optical properties.[1−6] For example, these monolayers can be readily assembled together like "Lego blocks", without large lattice mismatch effects, due to the interplane van der Waals forces, which offer a convenient and flexible approach to design various devices.[7] In addition, TMDs can be integrated into photonic devices such as modulators, detectors, and optical microcavities.[8−12] Furthermore, the high mobility and the tunable bandgap of these materials enables them to be versatile components for electrical and optical circuits.[13−16]

Here we report a photoluminescence switching effect based on monolayer WSe_2 transistors and an observation of a large blue shift of the photoluminescence line up to 36 meV. The photoluminescence (PL) intensity of the WSe_2 element was tuned by applying vertical electric fields in a dual-gate geometry. A back-gate is used to apply an electric field from the bottom of the sample; a side-gate geometry and the electric double layer (EDL) gating method were used to maximize the electric field at the top interface of WSe_2. When a side-gate voltage is applied, ions within a solid polymer electrolyte accumulate at the interface of the WSe_2 and induced countercharges. This design has the benefit that the interface electric field occurs across an extremely small distance, leading to a large electric field ($>10^7$ V/cm) and high capacitance density (1−10 μF/cm^2).[17−19] Another advantage of using EDL gating with side-gate geometry is that it does not block observation from above the channel, as a conventional top gate does, and therefore allows direct PL measurements from the top, as well as convenient integration into optoelectronic devices such as photodetectors or photoemitters.[20]

RESULTS AND DISCUSSION

We fabricated monolayer WSe_2 field effect transistors (FETs) with two different types of the source materials, one which was exfoliated and the other grown by chemical vapor deposition (CVD). Figure 1(a) shows typical PL spectra carried out before and after capping with the electrolyte poly(ethylene oxide) (PEO):$CsClO_4$. The capping led to a 17-fold increase

Received: July 15, 2021
Accepted: December 6, 2021
Published: December 8, 2021

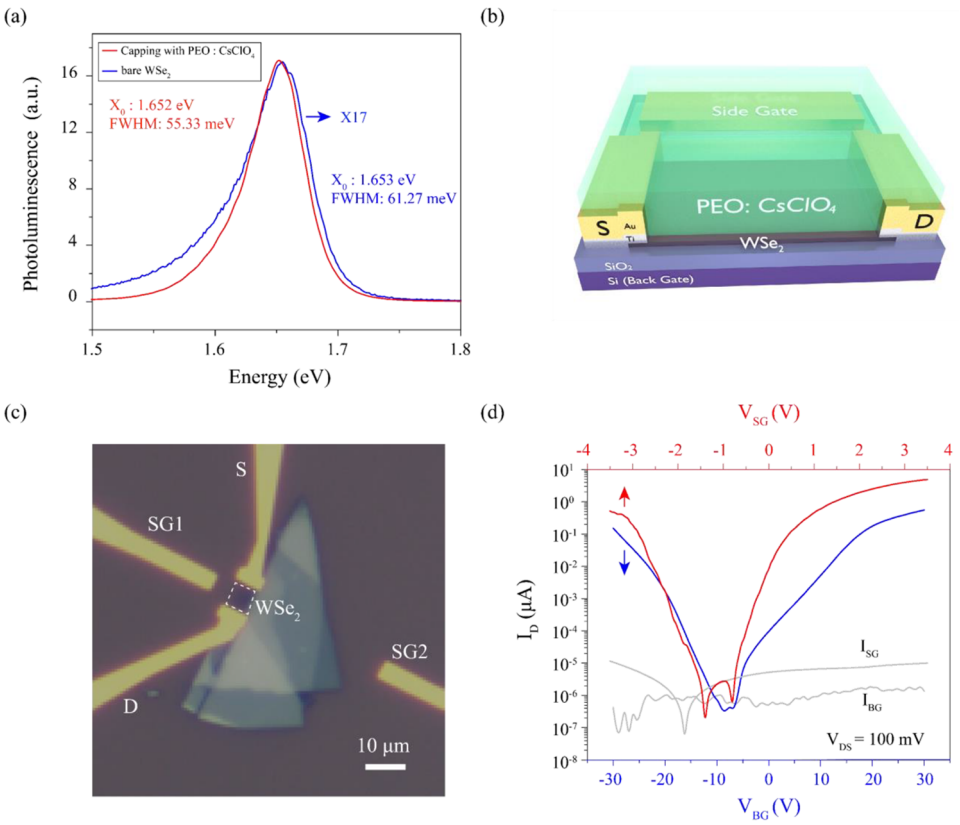

Figure 1. (a) Typical photoluminescence spectrum of the exfoliated monolayer WSe_2 with (red) and without (blue) capping PEO:$CsClO_4$. A factor of 17 enhancement was obtained after coating along with decreasing the line width from 61.27 meV to 55.33 meV. (b) Schematic of the WSe_2-based transistors. S is the source, D is the drain, SG1 is side-gate 1, and SG2 is side-gate 2 (which was not used for these studies). The source−drain channel length was about 10 μm. (c) Optical microscope image of the WSe_2-based transistor with two side-gates (SG2 was not used for these measurements). (d) Transfer characteristics of the FET before (blue) and after (red) depositing the PEO:$CsClO_4$ electrolyte. The back-gate scanning rate is 4 V/s and side-gate scanning rate is 10 mV/s. V_{DS} was kept at 100 mV. I_{SG} and I_{BG} are the leakage currents of the side-gate and the back-gate, respectively.

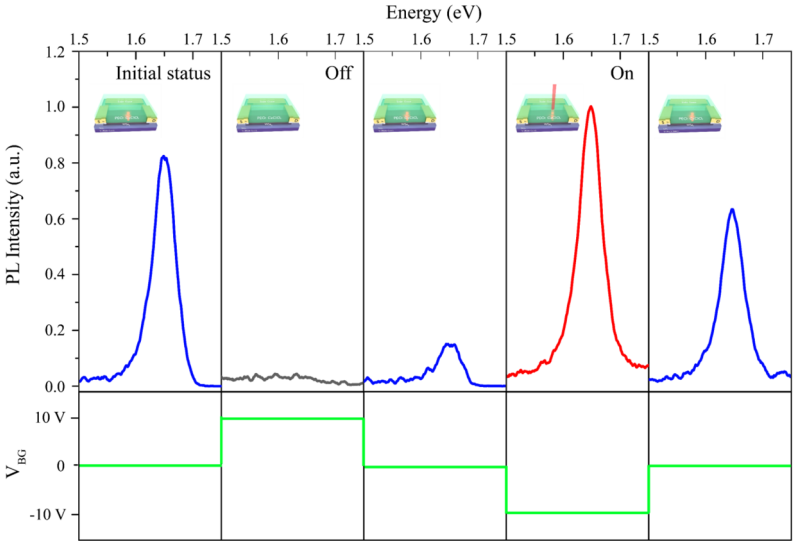

Figure 2. PL intensity in response to changing V_{BG} showing the switching effect. The top row is the PL spectra of the exfoliated WSe_2 transistor in response to a ±10 V back-gate voltage, shown at the bottom. The side-gate voltage is −2 V.

of the PL intensity and a narrowing of the full-width at half-maximum (fwhm) of 6 meV. The increase of the PL intensity may be explained by the motion of the ions to smooth the extrinsic disorder, for example, helping to neutralize charged impurities in the WSe_2.[21] The electrolyte coverage may also help to prevent the WSe_2 from oxidizing in the air.

For the first type of sample, an isolated monolayer, WSe_2, was mechanically exfoliated, with a typical size of 5 × 15 μm^2,

https://doi.org/10.1021/acsnano.1c06016
ACS Nano 2021, 15, 19439−19445

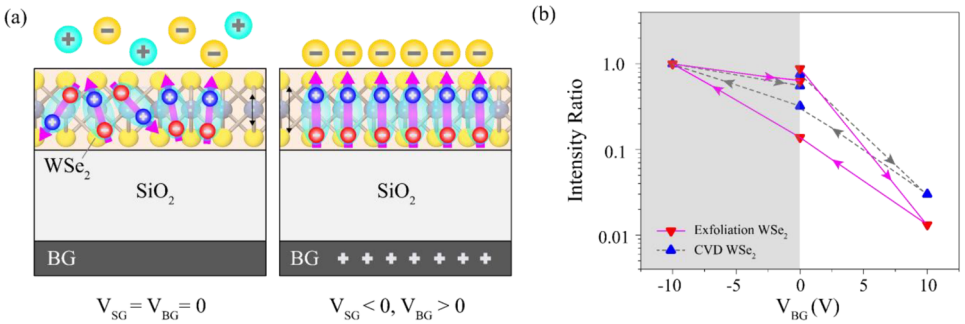

Figure 3. (a) Schematic of exciton dipole arrangements in the absence of an electric field (left) and with dual electric fields (right). Ions are randomly distributed if there is no voltage applied. When a negative V_{SG} is applied, anions accumulate near the channel, while cations (not shown) accumulate near the gate electrode, and the bulk part of the electrolyte remains charge neutral. (b) PL intensity of the exfoliated and CVD WSe_2-based transistors as a function of the back-gate voltage. The side-gate voltage was held at −2 V. The on/off ratios were 90 and 37, respectively. All the data points are normalized by the maximum intensity.

from which a transistor was made. Figure 1(b) illustrates the transistor design, and Figure 1(c) shows an optical microscope image. A similar device was made using a CVD-grown WSe_2 layer; the optical microscope image is shown in Supporting Information Figure S1. The results of three-terminal transfer measurements before and after depositing the electrolyte on the exfoliated sample are shown in Figure 1(d). A typical ambipolar transport behavior is observed in the transistor based on exfoliated WSe_2, suggesting that electrons and the holes can both be accumulated depending on the polarity of the applied gate voltage. The CVD-grown WSe_2 was p-doped, with only the hole-conduction branch observable in back-gate transfer measurements prior to the deposition of electrolyte (see Figure S2). As seen in Figure 1(d), using the electrolyte (red line) gave a 10-fold increase in the "On" current (n-branch), with only 1/10 of the applied voltage, thanks to the formation of the EDL and the resulting larger interface electric field.

After the initial optical and electrical characterization, we then performed gate-voltage-dependent PL measurements on the exfoliation sample. To investigate the gate-voltage dependence of the PL, we first applied −2 V on the side-gate (SG1) and monitored the change of the WSe_2 channel conductance with a small (100 mV) drain terminal voltage, while the source terminal was grounded. In response to the gate electric field, the cations and the anions within the electrolyte redistribute.[22,23] The channel conductance increased during this time as a result of the increase of the charge carriers (*i.e.*, holes) in the WSe_2 layer. After the ions reach equilibrium, we then performed the PL measurements and monitored the PL intensity variations as we tuned the back-gate voltage. All the measurements were performed in an ambient atmosphere at room temperature.

Figure 2 shows an unambiguous switching behavior, in which the PL intensity is turned off and turned on by modifying the back-gate voltages. PL intensity on/off ratios of 90 and 37 were observed in the exfoliated and CVD-grown samples, respectively, under the same conditions (the data for the CVD device are shown in the Supporting InformationFigure S3). For each voltage, we hold the voltage for 1 min before PL measurements to allow the device to reach equilibrium. The difference of PL intensity between initial, third, and fifth PL measurements with zero back-gate voltage can potentially be attributed to the lagging effect of exciton dipoles responding to external electric fields. After removing the back-gate voltage the exciton dipoles require time to relax to an equilibrium state, and each dipole's final alignment directions may not be the same as its initial direction. The relationship between exciton dipole directions and PL intensity is discussed later in this study.

Figure 3(a) is a schematic of device geometry and exciton dipole arrangements in the absence of electric field (left) and with dual electric fields (right), and Figure 3(b) shows the PL intensity as the function of the gate voltage in both exfoliated and CVD devices. In these measurements, the side-gate was held at −2 V and the back-gate was swept in the range of [−10, 10]. Both samples show the switching effect. The on/off ratio was determined to be 90 and 37 for the exfoliated and CVD-grown samples, respectively. When the polarity of the side-gate voltage was reversed, the on/off effect can still be observed by tuning the V_{BG}, but the on/off ratio decreased, as shown in the Supporting Information Figure S4. A control experiment was carried out to investigate the effect of removing the electric field from the bottom-gate in the CVD-grown sample and only applying the side-gate voltage. As expected, the change of the PL intensity was still observed under the single side-gate conditions, but the on/off ratio was reduced to 12 (Figure S3). This indicates that the PL switching effect is stronger when a vertical electric field is applied on both the side gate and back gate.

The PL intensity modulation *via* the gate voltage can be understood as follows. Initially, the excitons in the WSe_2 and the ions within the electrolyte are randomly distributed spatially, as illustrated in Figure 3(a). The applied negative side-gate voltage causes anion accumulation at the interface of the electrolyte and WSe_2. In addition to inducing more holes in the WSe_2, the anions can also attract holes moving toward the top interface while repelling electrons and moving them in the opposite direction. When a positive back-gate voltage is applied, the separation of the electron and the hole in an exciton is increased, as the positive back-gate pulls the electron toward the bottom and pushes the hole toward the top of the WSe_2 layer. The further the electron and the hole are separated spatially, the smaller the overlap of their wave function and the lower the probability of their recombination. Hence, the PL intensity can be turned off when the two gates possess the opposite polarity. However, it is turned back on when the polarity of the two gates is tuned to be the same, as there is no longer a force separating the electron and hole pairs within the excitons.

https://doi.org/10.1021/acsnano.1c06016
ACS Nano 2021, 15, 19439−19445

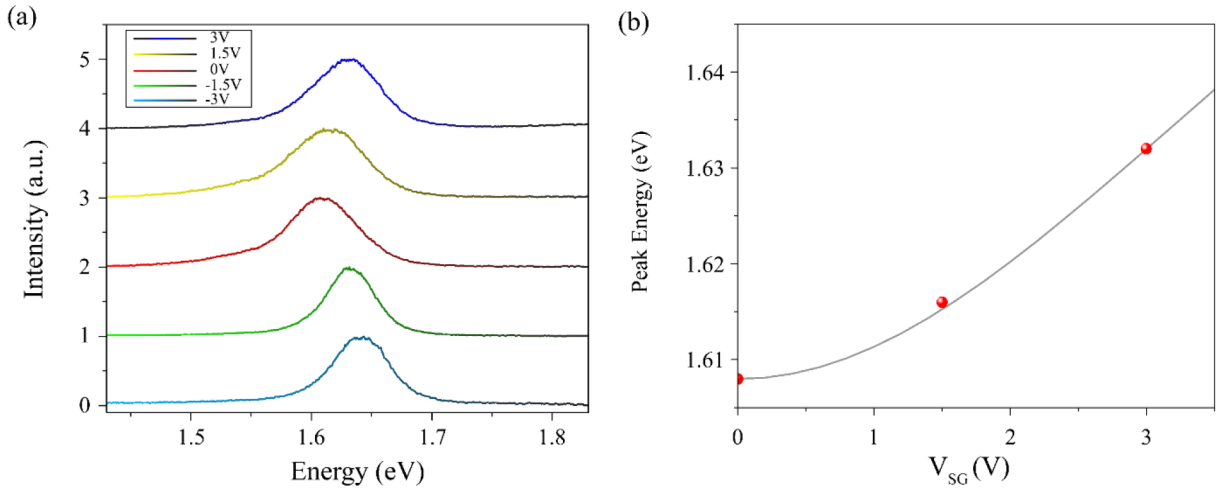

Figure 4. (a) PL spectra as a function of the side-gate voltage of the CVD-grown WSe_2-based transistor. The back-gate was grounded. The exciton energy can be determined by fitting the spectra with the Lorentzian model, and $|\Delta E_{max}|$ = 36 meV is obtained. (b) Peak energy (red dots) of the spectra for the positive polar side-gate overlaid with the calculation (gray line).

Additionally, when the two gates have the same polarity, they induce the same type of charges in the WSe_2 (*e.g.*, holes when $V_{SG} < 0$ V and $V_{BG} < 0$ V), leading to a higher doping density than with only one gate applied (*e.g.*, $V_{SG} < 0$ and $V_{BG} = 0$ V). As a result, surface charges can be filled, which reduces the nonradioactive relaxation channels and enhances the PL intensity.[21]

The variation of the PL intensity may also be understood from the change of the population of the excitons that are aligned along the out-of-plane direction. Emission from excitons with dipole moment in the out-of-plane direction is optically forbidden; these excitons are known as "dark" excitons.[24] The dipoles within the WSe_2 layer are affected by both the EDL at the electrolyte/WSe_2 interface and the back-gate. When an anionic EDL is formed at the WSe_2 interface and at the same time a positive back-gate is applied, a unipolar vertical electric field is formed in the monolayer WSe_2. It will cause the dipoles in the WSe_2 to become vertically aligned and therefore inhibit the emission in the out-of-plane direction. Reversing the polarity of the back-gate voltage changes the direction of the dipoles and thus reduces the populations of the dark excitons in the system. Hence, the PL intensity recovers.

The single- and dual-gate measurements on the CVD-grown sample helped test our hypothesis that the PL intensity is strongly affected by the magnitude (Figure S3) and direction of the applied electric field (Figure S4). As mentioned above, the on/off ratio increased from 12 to 37 when an additional gate with the same vertical electric field direction was applied. Comparing the dual-gate measurements on CVD-grown and exfoliated samples, the CVD-grown sample has a smaller on/off ratio (37) compared to the exfoliated one (90), which may indicate that the CVD sample contains more impurities than the exfoliated sample. The defects and the impurities in the CVD-grown sample can help to bind the carriers from being polarized.

Note that in the voltage range used in this study, the charging time of the EDL in the polymer electrolyte is tens to hundreds of seconds;[22] therefore, it would be challenging to conduct a gate-dependent transient PL measurement in this setup. However, our previous study shows that it is possible to reduce the EDL formation time constant to microseconds (or even nanoseconds based on modeling)[22] with significant reduction of device size, which is a potential pathway to better understand the charge carrier dynamics in this type of system. Also to be noted is that because an EDL will form at both the electrolyte−SiO_2 interface and the electrolyte−WSe_2 channel interface, there is some capacitive coupling effect. However, results from finite element modeling using COMSOL Multiphysics (shown in Figure S5) suggest that capacitive coupling from the nearby oxide does not play a significant role in EDL ion density.

We also observed a large Stark shift (blue shift) by controlling the side-gate voltage. This Stark shift was quite different depending on whether the WSe_2 layer was exfoliated or CVD grown. The exciton energy of the exfoliated sample does not show an obvious change in response to the electric field, but the CVD-grown sample shows significant modulation, as shown in Figure 4(a). The gate-voltage-dependent blue shift in this case was about 36 meV, which is the largest tunability of this line reported so far.[13,25] The exciton energy in this device shifted upward on both voltage polarities, but by different amounts, which may suggest different surface electric field magnitude. Although different ionic species accumulate at the channel top interface under different polarities (*i.e.*, a cationic EDL forms at $V_{SG} > 0$ V while an anionic EDL forms at $V_{SG} < 0$ V), we do not anticipate a change in surface electric field magnitude because our previous experimental results using Hall effect measurements, transfer measurement,[23,26] and simulation results using finite element modeling[27] suggest that the cationic and anionic EDLs have very similar densities. Thus, the shift may be related to the different times required for exciton dipoles to be realigned to a new direction, but more experiments and devices are needed, and answering this question is beyond the scope of this study.

The quantum-confined Stark effect in a quantum well can be described by the simple relationship $\Delta E \propto E^2 d_{QW}^4$,[28,29] where E is electric field strength and the d_{QW} is the thickness of the quantum well. The quantum-confined Stark effect gives a red shift due to the applied electric field. Although the electric field can approach 10^7 V/cm in our system, due to small thickness of the monolayer WSe_2, the electric field should not produce a significant red shift. Similarly, the effect of the wave function distortion in the vertical direction due to the electric field is also negligible, even though it plays a key role in the shift of

https://doi.org/10.1021/acsnano.1c06016
ACS Nano 2021, 15, 19439−19445

exciton energy in quantum wells.[30] As discussed above, we have observed a large blue shift of 36 meV in the devices with CVD-grown material. We attribute this blue shift to the nonlinear effect on the in-plane dielectric constant $\epsilon_{\parallel}$ due to the large vertical electric field $E_{\perp}$. In general, the dielectric constant can be expressed as $\epsilon_{\parallel} = \epsilon_0(1 + \chi^{(1)} + \chi^{(2)}E_{\perp} + \chi^{(3)}E_{\perp}^2 + ...)$, where $\chi^{(n)}$, n = 1, 2, 3, stands for the nth order (off-diagonal) optical susceptibilities. Note that the interaction between the electron and hole has a strong dependence on the in-plane dielectric constant due to the screening effect, which in turn modifies the exciton binding energy. Theoretically, this interaction can be modeled by a Keldysh potential:[31−36] $V_K(r) = -\frac{e^2}{8\epsilon_0 r_0}\left[H_0\left(\frac{\kappa r}{r_0}\right) - Y_0\left(\frac{\kappa r}{r_0}\right)\right]$. Here H_0 and Y_0 are the Struve and Bessel functions of the second kind and the screening length $r_0 = (\epsilon_{\parallel} - 1)d/2$ (with d = 0.658 nm being the thickness of the monolayer) largely depends on the dielectric constant. Furthermore, the value of linear susceptibility $\chi^{(1)} \approx 14$ for WSe_2 is known in the literature[34,36,37] and the second-order nonlinear susceptibility $\chi^{(2)}$ can be ignored in a uniform medium.[38] Therefore, the lowest-order nonlinear effect is attributed to the third-order optical susceptibility $\chi^{(3)}$, which can be determined by numerically calculating the exciton binding energy and fitting its change with respect to the perpendicular electric field $E_{\perp}$. Our result shows $\chi^{(3)} = 3.50 \times 10^{-19}$ m^2/V^2, which is the same order as the third-order *diagonal* susceptibility measured in others' experimental work[39] (refer to the Supporting Information for details). In Figure 4(b), we present the measured PL peak energy along with the theoretically calculated exciton energy as a function of the side-gate voltage. The calculated exciton energy is shifted by a constant in order to match the measured PL peak at zero electric field.

CONCLUSIONS

Transistors made with WSe_2 of two different types show a strong switching of the PL intensity under the applied electric field. The mechanism of the intensity variation can be attributed to the change of the background effective doping density and the direction of the dipole moment of the excitons as the electric field is varied. This effect may be useful for photonic applications; future work on this system should include detailed studies of the time-dependent behavior to determine the switching speed.

The large modulation of the exciton energy can be explained by the nonlinear effect on the in-plane dielectric constant induced by the vertical electric field. This strong shift may be of benefit when embedding TMD monolayers inside microcavities to make exciton-polaritons, which have great promise for photonic devices and Bose−Einstein condensation of exciton-polaritons at room temperature. In general, exciton-polaritons in microcavities are highly sensitive to the exact detuning of the exciton and cavity photon energies, and having direct, electrical control over the detuning provides a very useful design element. While the large binding energy and the strong oscillator strength[40,41] of the excitons in TMD materials are well known, the large tunability of the exciton properties seen here raises many possibilities for all-optical devices at room temperature in the future.[42]

METHODS

Device Fabrication. An isolated monolayer WSe_2 with a typical size of 5 × 15 μm^2 was mechanically exfoliated from bulk crystals (purchased from 2D Semiconductors). The whole sample was fabricated by the standard dry transferring method to the surface of a p-doped silicon substrate with 90 nm SiO_2 coating (purchased from the Graphene Supermarket). Two contacts were written on top of the flake *via* e-beam lithography, to give a parallel electric field to the surface as the source (S) and drain (D); two side leads were written off the flake for applying the side-gate (SG) voltage. This was followed by an e-beam deposition of Ti/Au 3/100 nm. The metal was grown at a pressure of 10^{-6} Torr. We made a similar device on a CVD-grown sample (material provided by 2DLayer).

Electrolyte Preparation. The dual-ion conducting polymer electrolyte (PEO:$CsClO_4$) was prepared similarly to previously published work.[26] PEO (Polymer Standards Service, M_w = 94 600 g mol^{-1}) and $CsClO_4$ (Sigma-Aldrich, 99.9%) were dissolved in anhydrous acetonitrile (Sigma-Aldrich) to make a 1 wt % solution with an ether oxygen to Cs molar ratio of 20:1 (concentration of salt in PEO is 1177 mol/m^3).

Optical Measurements. A He−Ne laser with a spot size of 1 μm at normal incidence through an 50× Mitutoyo microscope objective was employed as the pump source. The PL spectra were collected by the same microscope objective and directed toward a charged couple device (CCD) equipped spectrometer.

Electronic Characterization. A Keysight B1500A semiconductor parameter analyzer in a Lakeshore cryogenic vacuum probe station (CRX-VF) at a pressure of 2 × 10^{-6} Torr is exploited. For the transfer measurements in Figure 1 the scanning rate is 4 V/s for the back-gate and 10 mV/s for the side-gate. V_{DS} was 100 mV for both measurements.

ASSOCIATED CONTENT

Supporting Information

The Supporting Information is available free of charge at https://pubs.acs.org/doi/10.1021/acsnano.1c06016.

Optical and electrical characterizations of the as-fabricated device; single- and dual-gated PL measurements; optical switching effect for different polarity, for CVD-grown WSe_2 sample; theory for nonlinear optical susceptibility and the blue shift of PL energy; finite element simulation for capacitive coupling effect from electrolyte/oxide interface by COMSOL (PDF)

AUTHOR INFORMATION

Corresponding Author

Zheng Sun − *State Key Laboratory of Precision Spectroscopy, East China Normal University, Shanghai 200241, China; Department of Physics and Astronomy, University of Pittsburgh, Pittsburgh, Pennsylvania 15260, United States;* orcid.org/0000-0002-5209-2563; Email: zsun@lps.ecnu.edu.cn

Authors

Ke Xu − *Department of Chemical and Petroleum Engineering, University of Pittsburgh, Pittsburgh, Pennsylvania 15260, United States; School of Physics and Astronomy, Rochester Institute of Technology, Rochester, New York 14623, United States; Microsystems Engineering, Rochester Institute of Technology, Rochester, New York 14623, United States;* orcid.org/0000-0003-2692-1935

Chang Liu − *State Key Laboratory of Precision Spectroscopy, East China Normal University, Shanghai 200241, China; Institute for Advanced Study, Tsinghua University, Beijing 100084, China*

Jonathan Beaumariage − *Department of Physics and Astronomy, University of Pittsburgh, Pittsburgh, Pennsylvania 15260, United States*

Jierui Liang − *Department of Physics and Astronomy, University of Pittsburgh, Pittsburgh, Pennsylvania 15260, United States;* orcid.org/0000-0003-1207-8959

Susan K. Fullerton-Shirey − *Department of Chemical and Petroleum Engineering, University of Pittsburgh, Pittsburgh, Pennsylvania 15260, United States;* orcid.org/0000-0003-2720-0400

Zhe-Yu Shi − *State Key Laboratory of Precision Spectroscopy, East China Normal University, Shanghai 200241, China*

Jian Wu − *State Key Laboratory of Precision Spectroscopy, East China Normal University, Shanghai 200241, China; Collaborative Innovation Center of Extreme Optics, Shanxi University, Taiyuan, Shanxi 030006, China; CAS Center for Excellence in Ultra-intense Laser Science, Shanghai 201800, China*

David Snoke − *Department of Physics and Astronomy, University of Pittsburgh, Pittsburgh, Pennsylvania 15260, United States*

Complete contact information is available at: https://pubs.acs.org/10.1021/acsnano.1c06016

Author Contributions

[#]Z.S., K.X., and C.L. contributed equally to this work.

Notes

The authors declare no competing financial interest.

ACKNOWLEDGMENTS

Z.S. acknowledges support from the NSFC Grant No. 12174111, Shanghai Pujiang Program Grant No. 21PJ1403000, and Joint Physics Research Institute Challenge Grant of the NYU-ECNU Institute of Physics at NYU Shanghai. This work was also supported by the U.S. Army Research Office under MURI Award No. W911NF-17-1-0312 (Z.S., J.B., and D.S.). K.X., J.L., and S.K.F.-S. acknowledge funding from NSF-DMR-EPM grant #1607935 and helpful discussions with Brendan Mostek and Shubham Awate. Z.-Y.S. acknowledges support from Program of Shanghai Sailing Program Grant No. 20YF1411600 and NSFC Grant No. 12004115. J.W. acknowledges the support from the National Key R&D Program of China (Grant No. 2018YFA0306303), Shanghai Municipal Science and Technology Major Project.

REFERENCES

(1) Mak, K. F.; Shan, J. Photonics and Optoelectronics of 2D Semiconductor Transition Metal Dichalcogenides. *Nat. Photonics* **2016**, *10* (4), 216−226.

(2) Xia, F.; Wang, H.; Xiao, D.; Dubey, M.; Ramasubramaniam, A. Two-Dimensional Material Nanophotonics. *Nat. Photonics* **2014**, *8* (12), 899−907.

(3) Wang, Q. H.; Kalantar-Zadeh, K.; Kis, A.; Coleman, J. N.; Strano, M. S. Electronics and Optoelectronics of Two-Dimensional Transition Metal Dichalcogenides. *Nat. Nanotechnol.* **2012**, *7* (11), 699−712.

(4) Butler, S. Z.; Hollen, S. M.; Cao, L.; Cui, Y.; Gupta, J. A.; Gutiérrez, H. R.; Heinz, T. F.; Hong, S. S.; Huang, J.; Ismach, A. F.; Johnston-Halperin, E.; Kuno, M.; Plashnitsa, V. V.; Robinson, R. D.; Ruoff, R. S.; Salahuddin, S.; Shan, J.; Shi, L.; Spencer, M. G.; Terrones, M.; Windl, W.; Goldberger, J. E. Progress, Challenges, and Opportunities in Two-Dimensional Materials beyond Graphene. *ACS Nano* **2013**, *7* (4), 2898−2926.

(5) Xu, X.; Yao, W.; Xiao, D.; Heinz, T. F. Spin and Pseudospins in Layered Transition Metal Dichalcogenides. *Nat. Phys.* **2014**, *10* (5), 343−350.

(6) Galfsky, T.; Sun, Z.; Considine, C. R.; Chou, C.-T.; Ko, W.-C.; Lee, Y.-H.; Narimanov, E. E.; Menon, V. M. Broadband Enhancement of Spontaneous Emission in Two-Dimensional Semiconductors Using Photonic Hypercrystals. *Nano Lett.* **2016**, *16* (8), 4940.

(7) Geim, A. K.; Grigorieva, I. V. van der Waals Heterostructures. *Nature* **2013**, *499* (7459), 419−425.

(8) Liu, X.; Galfsky, T.; Sun, Z.; Xia, F.; Lin, E. C.; Lee, Y. H.; Kéna-Cohen, S.; Menon, V. M. Strong Light-Matter Coupling in Two-Dimensional Atomic Crystals. *Nat. Photonics* **2015**, *9* (1), 30−34.

(9) Sun, Z.; Gu, J.; Ghazaryan, A.; Shotan, Z.; Considine, C. R.; Dollar, M.; Chakraborty, B.; Liu, X.; Ghaemi, P.; Kéna-Cohen, S.; Menon, V. M. Optical Control of Roomerature Valley Polaritons. *Nat. Photonics* **2017**, *11* (8), 491−496.

(10) Wu, E.; Xie, Y.; Zhang, J.; Zhang, H.; Hu, X.; Liu, J.; Zhou, C.; Zhang, D. Dynamically Controllable Polarity Modulation of MoTe2 Field-Effect Transistors through Ultraviolet Light and Electrostatic Activation. *Sci. Adv.* **2019**, *5* (5), 1−10.

(11) Hu, Y.; Huang, Y.; Tan, C.; Zhang, X.; Lu, Q.; Sindoro, M.; Huang, X.; Huang, W.; Wang, L.; Zhang, H. Two-Dimensional Transition Metal Dichalcogenide Nanomaterials for Biosensing Applications. *Mater. Chem. Front.* **2017**, *1* (1), 24−36.

(12) Chakraborty, B.; Gu, J.; Sun, Z.; Khatoniar, M.; Bushati, R.; Boehmke, A. L.; Koots, R.; Menon, V. M. Control of Strong Light-Matter Interaction in Monolayer WS2 through Electric Field Gating. *Nano Lett.* **2018**, *18* (10), 6455−6460.

(13) Sun, Z.; Beaumariage, J.; Xu, K.; Liang, J.; Hou, S.; Forrest, S. R.; Fullerton-Shirey, S. K.; Snoke, D. W. Electric-Field-Induced Optical Hysteresis in Single-Layer WSe_2. *Appl. Phys. Lett.* **2019**, *115* (16), 161103.

(14) Sun, Z.; Beaumariage, J.; Movva, H. C. P.; Chowdhury, S.; Roy, A.; Banerjee, S. K.; Snoke, D. W. Stress-Induced Bandgap Renormalization in Atomic Crystals. *Solid State Commun.* **2019**, *288*, 18−21.

(15) Johari, P.; Shenoy, V. B. Tuning the Electronic Properties of Semiconducting Transition Metal Dichalcogenides by Applying Mechanical Strains. *ACS Nano* **2012**, *6* (6), 5449−5456.

(16) Feng, J.; Qian, X.; Huang, C. W.; Li, J. Strain-Engineered Artificial Atom as a Broad-Spectrum Solar Energy Funnel. *Nat. Photonics* **2012**, *6* (12), 866−872.

(17) Ye, J. T.; Zhang, Y. J.; Akashi, R.; Bahramy, M. S.; Arita, R.; Iwasa, Y. Superconducting Dome in a Gate-Tuned Band Insulator. *Science* **2012**, *338* (6111), 1193−1196.

(18) Bisri, S. Z.; Shimizu, S.; Nakano, M.; Iwasa, Y. Endeavor of Iontronics: From Fundamentals to Applications of Ion-Controlled Electronics. *Adv. Mater.* **2017**, *29* (25), 1−48.

(19) Xu, K.; Fullerton-Shirey, S. K. Electric-Double-Layer-Gated Transistors Based on Two-Dimensional Crystals: Recent Approaches and Advances. *J. Phys. Mater.* **2020**, *3* (3), 032001.

(20) Li, Z.; Chang, S. W.; Chen, C. C.; Cronin, S. B. Enhanced Photocurrent and Photoluminescence Spectra in MoS2 under Ionic Liquid Gating. *Nano Res.* **2014**, *7* (7), 973−980.

(21) Rhodes, D.; Chae, S. H.; Ribeiro-Palau, R.; Hone, J. Disorder in van der Waals Heterostructures of 2D Materials. *Nat. Mater.* **2019**, *18* (6), 541−549.

(22) Xu, K.; Islam, M. M.; Guzman, D.; Seabaugh, A. C.; Strachan, A.; Fullerton-Shirey, S. K. Pulse Dynamics of Electric Double Layer Formation on All-Solid-State Graphene Field-Effect Transistors. *ACS Appl. Mater. Interfaces* **2018**, *10* (49), 43166−43176.

(23) Li, H. M.; Xu, K.; Bourdon, B.; Lu, H.; Lin, Y. C.; Robinson, J. A.; Seabaugh, A. C.; Fullerton-Shirey, S. K. Electric Double Layer Dynamics in Poly(ethylene oxide) LiClO4 on Graphene Transistors. *J. Phys. Chem. C* **2017**, *121* (31), 16996−17004.

(24) Zhou, Y.; Scuri, G.; Wild, D. S.; High, A. A.; Dibos, A.; Jauregui, L. A.; Shu, C.; De Greve, K.; Pistunova, K.; Joe, A. Y.; Taniguchi, T.; Watanabe, K.; Kim, P.; Lukin, M. D.; Park, H. Probing Dark Excitons in Atomically Thin Semiconductors *via* Near-Field

Coupling to Surface Plasmon Polaritons. *Nat. Nanotechnol.* **2017**, *12* (9), 856−860.
(25) Matsuki, K.; Pu, J.; Kozawa, D.; Matsuda, K.; Li, L. J.; Takenobu, T. Effects of Electrolyte Gating on Photoluminescence Spectra of Large-Area WSe_2 Monolayer Films. *Jpn. J. Appl. Phys.* **2016**, *55* (6), 06GB02.
(26) Xu, K.; Liang, J.; Woeppel, A.; Bostian, M. E.; Ding, H.; Chao, Z.; McKone, J. R.; Beckman, E. J.; Fullerton-Shirey, S. K. Electric Double-Layer Gating of Two-Dimensional Field-Effect Transistors Using a Single-Ion Conductor. *ACS Appl. Mater. Interfaces* **2019**, *11* (39), 35879−35887.
(27) Woeppel, A.; Xu, K.; Kozhakhmetov, A.; Awate, S.; Robinson, J. A.; Fullerton-Shirey, S. K. Single- *versus* Dual-Ion Conductors for Electric Double Layer Gating: Finite Element Modeling and Hall-Effect Measurements. *ACS Appl. Mater. Interfaces* **2020**, *12* (36), 40850−40858.
(28) Bastard, G.; Mendez, E. E.; Chang, L. L.; Esaki, L. Variational Calculations on a Quantum Well in an Electric Field. *Phys. Rev. B: Condens. Matter Mater. Phys.* **1983**, *28* (6), 3241−3245.
(29) Singh, J. *Electronic and Optoelectronic Properties of Semiconductor Structures [Book Review]*. Cambridge University Press: London, 2003, DOI: 10.1017/CBO9780511805745.
(30) Szymanska, M. H.; Littlewood, P. B. Excitonic Binding in Coupled Quantum Wells. *Phys. Rev. B: Condens. Matter Mater. Phys.* **2003**, *67* (19), 3−6.
(31) Stier, A. V.; Wilson, N. P.; Velizhanin, K. A.; Kono, J.; Xu, X.; Crooker, S. A. Magnetooptics of Exciton Rydberg States in a Monolayer Semiconductor. *Phys. Rev. Lett.* **2018**, *120* (5), 1−6.
(32) Keldysh, L. V. Coulomb Interaction in Thin Semiconductor and Semimetal Films. *JETP Lett.* **1979**, 658−661.
(33) Cudazzo, P.; Tokatly, I. V.; Rubio, A. Dielectric Screening in Two-Dimensional Insulators: Implications for Excitonic and Impurity States in Graphane. *Phys. Rev. B: Condens. Matter Mater. Phys.* **2011**, *84* (8), 1−7.
(34) Berkelbach, T. C.; Hybertsen, M. S.; Reichman, D. R. Theory of Neutral and Charged Excitons in Monolayer Transition Metal Dichalcogenides. *Phys. Rev. B: Condens. Matter Mater. Phys.* **2013**, *88* (4), 1−6.
(35) Wu, F.; Qu, F.; Macdonald, A. H. Exciton Band Structure of Monolayer MoS2. *Phys. Rev. B: Condens. Matter Mater. Phys.* **2015**, *91* (7), 1−8.
(36) Kylänpää, I.; Komsa, H. P. Binding Energies of Exciton Complexes in Transition Metal Dichalcogenide Monolayers and Effect of Dielectric Environment. *Phys. Rev. B: Condens. Matter Mater. Phys.* **2015**, *92* (20), 1−6.
(37) Stier, A. V.; Wilson, N. P.; Clark, G.; Xu, X.; Crooker, S. A. Probing the Influence of Dielectric Environment on Excitons in Monolayer WSe2: Insight from High Magnetic Fields. *Nano Lett.* **2016**, *16* (11), 7054−7060.
(38) Boyd, R. W. *Nolinear Optics*; Elsevier: Amsterdam, 1967.
(39) Autere, A.; Jussila, H.; Marini, A.; Saavedra, J. R. M.; Dai, Y.; Säynätjoki, A.; Karvonen, L.; Yang, H.; Amirsolaimani, B.; Norwood, R. A.; Peyghambarian, N.; Lipsanen, H.; Kieu, K.; De Abajo, F. J. G.; Sun, Z. Optical Harmonic Generation in Monolayer Group-VI Transition Metal Dichalcogenides. *Phys. Rev. B: Condens. Matter Mater. Phys.* **2018**, *98* (11), 1−7.
(40) Qiu, D. Y.; Da Jornada, F. H.; Louie, S. G. Optical Spectrum of MoS2: Many-Body Effects and Diversity of Exciton States. *Phys. Rev. Lett.* **2013**, *111* (21), 1−5.
(41) Chernikov, A.; Berkelbach, T. C.; Hill, H. M.; Rigosi, A.; Li, Y.; Aslan, O. B.; Reichman, D. R.; Hybertsen, M. S.; Heinz, T. F. Exciton Binding Energy and Nonhydrogenic Rydberg Series in Monolayer WS2. *Phys. Rev. Lett.* **2014**, *113* (7), 1−5.
(42) Sun, Z.; Snoke, D. W. Optical Switching with Organics. *Nat. Photonics* **2019**, *13* (June), 370−371.

https://doi.org/10.1021/acsnano.1c06016
ACS Nano 2021, 15, 19439−19445